Acta Pharmaceutica Sinica B 2024;14(6):2537–2553

Chinese Pharmaceutical Association
Institute of Materia Medica, Chinese Academy of Medical Sciences

Acta Pharmaceutica Sinica B

www.elsevier.com/locate/apsb
www.sciencedirect.com

ORIGINAL ARTICLE

Transient induction of actin cytoskeletal remodeling associated with dedifferentiation, proliferation, and redifferentiation stimulates cardiac regeneration

Wenbin Fu[a,b,c], Qiao Liao[a,b,c], Yu Shi[a,b,c], Wujian Liu[a,b,c], Hongmei Ren[a,b,c], Chunmei Xu[a,b,c], Chunyu Zeng[a,b,c,d,e,f,*]

[a]*Department of Cardiology, Daping Hospital, the Third Military Medical University (Army Medical University), Chongqing 400042, China*
[b]*Key Laboratory of Geriatric Cardiovascular and Cerebrovascular Disease Research, Ministry of Education of China, Chongqing 400042, China*
[c]*Chongqing Key Laboratory for Hypertension Research, Chongqing Cardiovascular Clinical Research Center, Chongqing Institute of Cardiology, Chongqing 400042, China*
[d]*State Key Laboratory of Trauma, Burns and Combined Injury, Daping Hospital, the Third Military Medical University, Chongqing 400042, China*
[e]*Cardiovascular Research Center, Chongqing College, University of Chinese Academy of Sciences, Chongqing 400042, China*
[f]*State Key Laboratory of Trauma and Chemical Poisoning, Chongqing 400042, China*

Received 2 November 2023; received in revised form 3 January 2024; accepted 5 January 2024

KEY WORDS

Single cell analysis;
Actin remodeling;
Tmsb4x;
Tmsb10;
Dmd;
Ctnna3;

Abstract The formation of new and functional cardiomyocytes requires a 3-step process: dedifferentiation, proliferation, and redifferentiation, but the critical genes required for efficient dedifferentiation, proliferation, and redifferentiation remain unknown. In our study, a circular trajectory using single-nucleus RNA sequencing of the pericentriolar material 1 positive ($PCM1^{+}$) cardiomyocyte nuclei from hearts 1 and 3 days after surgery-induced myocardial infarction (MI) on postnatal Day 1 was reconstructed and demonstrated that actin remodeling contributed to the dedifferentiation, proliferation, and redifferentiation of cardiomyocytes after injury. We identified four top

*Corresponding author.
E-mail addresses: chunyuzeng01@163.com, zengchunyu@tmmu.edu.cn (Chunyu Zeng).

Peer review under the responsibility of Chinese Pharmaceutical Association and Institute of Materia Medica, Chinese Academy of Medical Sciences.

https://doi.org/10.1016/j.apsb.2024.01.021

Myocardial infarction;
Cardiomyocytes proliferation;
Cardiac regeneration;
Genetic therapy

actin-remodeling regulators, namely *Tmsb4x*, *Tmsb10*, *Dmd*, and *Ctnna3*, which we collectively referred to as 2D2P. Transiently expressed changes of 2D2P, using a polycistronic non-integrating lentivirus driven by *Tnnt2* (cardiac-specific troponin T) promoters (Tnnt2-2D2P-NIL), efficiently induced transiently proliferative activation and actin remodeling in postnatal Day 7 cardiomyocytes and adult hearts. Furthermore, the intramyocardial delivery of Tnnt2-2D2P-NIL resulted in a sustained improvement in cardiac function without ventricular dilatation, thickened septum, or fatal arrhythmia for at least 4 months. In conclusion, this study highlights the importance of actin remodeling in cardiac regeneration and provides a foundation for new gene-cocktail-therapy approaches to improve cardiac repair and treat heart failure using a novel transient and cardiomyocyte-specific viral construct.

1. Introduction

Cardiomyocytes in mammals lose their regenerative capacity during early postnatal life. However, the heart in the first postnatal week of mice possesses a regenerative response that can restore the damaged heart to its normal anatomy and function following several types of injury[1,2]. This endogenous cardiac regeneration is primarily driven by pre-existing cardiomyocytes[3,4]. While immature cardiomyocytes produced by mere proliferation can only replenish the existing number of cardiomyocytes, the formation of new and functional cardiomyocytes must go through a 3-step process: dedifferentiation, proliferation, and redifferentiation[5]. The ability to control this process in the postnatal heart would represent a powerful approach for mammalian cardiac regeneration and myocardial infarction (MI) treatment, but the critical genes required for efficient dedifferentiation, proliferation, and redifferentiation remain unclear.

Recent studies have utilized single-nucleus RNA sequencing (snRNA-seq) to elucidate the dynamic transcriptional landscape of cardiomyocyte clusters in neonatal regenerating mouse hearts following MI injury[6]. We constructed the trajectory throughout the entire process to discover the essential components governing cardiac regeneration. The findings suggested that actin cytoskeletal remodeling may serve as the fundamental driver of change in sarcomeric structures. Moreover, the transient alteration of two depolymerization (2D) genes (*Tmsb4x* and *Tmsb10*) and two polymerization (2P) genes (*Dmd* and *Ctnna3*) can collectively contribute to the dedifferentiation, proliferation, and redifferentiation of cardiomyocytes.

Therapeutic gene products are used for treating many diseases, but they can be harmful if there is a lack of temporal and spatial control[7,8]. Adeno-associated virus-mediated expression of genes can stimulate cardiomyocyte proliferation, but the subsequently persistent and uncontrolled expression of genes may cause impairment of redifferentiation, leading to serious long-term consequences, such as fatal arrhythmia and sudden death[8]. To address this concern, we controlled the transient changes of 2D2P genes in the adult mouse heart to imitate the actin remodeling in the neonatal regenerating mouse heart after MI injury, using a non-integrating lentivirus (NIL). Moreover, the spatially expressed control of 2D2P genes was maximally guaranteed by cardiomyocyte-specific promoters and intramyocardial injection to avoid tumorigenesis. We found that transient changes in 2D2P genes effectively caused cardiomyocyte expansion, which was accompanied by actin remodeling and long-term improvement of cardiac function without adverse effects. Our study provided a foundation for new gene therapeutic approaches to improve cardiac repair and treat heart failure using a novel transient and cardiomyocyte-specific viral construct.

2. Methods and materials

2.1. Experimental animals

The present study utilized C57BL/6J mice and Sprague−Dawley rats as experimental models. The Institutional Animal Care and Use Committee approved the experimental protocol. All surgical procedures were performed under anesthesia, and measures were taken to minimize animal suffering. All experiments were carried out in accordance with the recommendations in the Guide for the Care and Use of Laboratory Animals of the National Institutes of Health.

2.2. Isolation and transfection of neonatal rat ventricular myocytes (NRVMs)

NRVMs were isolated from the hearts of less than 24-h-old Sprague−Dawley rats, as previously described[2]. Briefly, the ventricles of the rats were extracted and placed in a cold Ca^{+} and Mg^{+} free D-Hank's solution (Solarbio). After washing, the tissues were cut into pieces measuring approximately one cubic millimeter and digested with 1.25 mg/mL trypsin (Worthington) and 1.0 mg/mL collagenase II (Worthington). The isolated NRVMs were pre-plated for 2 h to remove fibroblasts. Subsequently, the cardiomyocytes were collected and cultured in 89% DMEM with 10% fetal bovine serum (FBS) and 1% penicillin−streptomycin (Gibco).

The sequences of siRNAs and saRNA used in this study are shown in Supporting Information Table S1 and a scrambled sequence was used as a negative control. The siRNA-*Dmd* was transfected into NRVMs using RNAiMAX (Invitrogen), following the manufacturer's instructions. Adenovirus (serotype 5) encoding saRNA-*Dmd* was purchased from Genechem (Shanghai, China), and cell infection was performed at a multiplicity of infection of 100. The siRNA-*Dmd* was transfected into NRVMs in the first

48 h, and after changing the culture medium, adenovirus infection was performed the following 48 h.

2.3. Isolation, purification, and transfection of neonatal mouse ventricular myocytes (NMVMs)

We isolated NMVMs from C57BL/6J mice on postnatal Day 7. The ventricles were extracted from mice and placed in a cold Ca^{+} and Mg^{+} free D-Hank's solution (Solarbio). The tissues were then cut into approximately one cubic millimeter pieces and digested using 1.25 mg/mL trypsin (Worthington) and 1.0 mg/mL collagenase II (Worthington). After pre-plating for 1 h to remove fibroblasts, the cell suspension was centrifuged using low- and high-density Percoll solutions[9]. Purified living cardiomyocytes were located at the interface of the low- and high-density gradients[9]. These cardiomyocytes were then washed and cultured in 89% DMEM with 10% FBS and 1% penicillin-streptomycin (Gibco). The concentration of verteporfin (a Yap inhibitor, MCE) treatment was 10 μmol/L.

To investigate the effects of *Tmsb4x* (or *Tmsb4x-mutant*), *Tmsb10* (or *Tmsb10-mutant*), shRNA-*Dmd*, and shRNA-*Ctnna3* on NMVMs, we used non-integrating lentiviruses encoding these genes with the Tnnt2 promoters and green fluorescent protein (GFP) reporter, which were obtained from Genechem (Shanghai, China). The cDNA sequences for these genes are shown in Table S1. Cell infection was performed at a multiplicity of infection of 100, following the manufacturer's instructions.

2.4. MI model

To induce MI in 8-week-old mice, we permanently ligated the left anterior descending (LAD) coronary artery, as previously described.[2] This procedure involved the opening of the fourth intercostal space under 2% isoflurane anesthesia, followed by suturing of the LAD with 7-0 silk, located 2−3 mm distal to the left atrial appendage. After 7 days of MI induction, the mice were re-anesthetized with 2% isoflurane, and the chest was reopened through the third intercostal space. The mice were randomly assigned to receive an intramyocardial injection of 30 μL, using a 32-gauge needle of either Tnnt2-2D2P-NIL or Control-NIL virus at three different sites (two sites at the infarct border zone and one site at the remote zone), with approximately 2×10^7 transducing units per mouse heart.

2.5. Adult cardiomyocyte isolation

To isolate adult cardiomyocytes, mice were subjected to an intraperitoneal injection of 100 μL heparin (6.25 U/μL) to prevent clotting. After a 30-min interval, the mice were anesthetized with 2% isoflurane, and their hearts were exposed and connected to a Langendorf perfusion system *via* an aortic cannula. The hearts were initially perfused with a perfusion buffer (140 mmol/L NaCl, 4 mmol/L KCl, 1 mmol/L $MgCl_2$, 10 mmol/L HEPES, 10 mmol/L taurine, 10 mmol/L 2,3-butanedione monoxime, and 10 mmol/L glucose at pH 7.3) for 5 min to eliminate residual blood. The hearts were then perfused with a digestion buffer (consisting of perfusion buffer containing 1 mg/mL collagenase II, 0.12 mg/mL trypsin, and 0.02 mmol/L $CaCl_2$) for 12−15 min until they were softened and collapsed. The digested hearts were transferred into a dish and minced with scissors. The minced hearts were then placed in a stop buffer (consisting of perfusion buffer containing 5 mg/mL bovine serum albumin and 0.1 mmol/L $CaCl_2$) to terminate the digestion. The isolated cells were filtered through a 100 μm strainer and centrifuged for 3 min at 50 × *g* to collect the cardiomyocytes, as previously described[2].

2.6. Echocardiographic evaluation and electrocardiogram recording

Echocardiography was conducted using a Vevo 3100 LT system (Visual Sonics) to evaluate cardiac morphology and function. The examination was performed by a skilled operator, and heart rates were maintained between 420 and 480 beats/min and adjusted by the inhalation of 0.5%−3% isoflurane. M-mode imaging was used in conjunction with the long-axis view to measure the left ventricular (LV) internal diameter during systole (LVIDs) and diastole (LVIDd). The LV ejection fraction (EF) was calculated using Eq. (1):

$$\mathrm{LVEF}\,(\%) = \left(\mathrm{LVIDd}^3 - \mathrm{LVIDs}^3\right) / \mathrm{LVIDd}^3 \times 100 \quad (1)$$

Additionally, the LV fraction shortening (FS) was calculated using Eq. (2):

$$\mathrm{LVFS}\,(\%) = (\mathrm{LVIDd} - \mathrm{LVIDs})/\mathrm{LVIDd} \times 100 \quad (2)$$

Three consecutive values were obtained and analyzed using Vevo LAB software. Electrocardiogram recording was conducted using the physiological index monitoring system on this instrument. To ensure blinding of a specific treatment, a random number was assigned to each mouse before the echocardiographic examinations.

2.7. Measurement of cardiac fibrosis

The hearts were rinsed with phosphate-buffered saline (PBS) and subsequently fixed in 4% paraformaldehyde at 4 °C overnight. Following three washes in PBS, the hearts were dehydrated in a PBS solution of 15% and 30% sucrose at 4 °C overnight and then embedded in optimum cutting tissue (Sakura). Cryosections of 10-μm thickness were obtained and stored at −20 °C until use.

The size of fibrosis caused by the infarct was measured by Masson's trichrome staining (Solarbio) or Sirius red staining. According to the manufacturer's protocols, the heart sections were stained with Masson trichrome stain. For Sirius red staining, the sections were fixed with Bouins' solution overnight and washed with tap water until the yellow color disappeared. Then sections were stained with Fast green for 3 min, followed by 1% acetic acid for 1 min and 0.1% Sirius red for 1−1.5 min. The myocardial midline of the left ventricle was drawn at the center between the epicardial and endocardial surfaces. Midline lengths of infarct and non-infarct walls in the left ventricle were measured in Fiji software. The percentage of fibrotic length indicating infarct ratio was calculated by dividing the infarct length by the total of the infarct and non-infarct lengths and then multiplying the result by 100[2].

2.8. Hematoxylin-eosin staining

The tissues of mice were cryo-sectioned and stained with an Hematoxylin−Eosin staining kit according to the manufacturer's protocols (Solarbio).

2.9. Immunofluorescence analysis

For immunostaining *in vitro*, NRVMs and NMVMs were first washed with PBS, followed by fixation with 4% paraformaldehyde and permeabilization with 0.1% Triton X-100 at room temperature. Subsequently, after treatment with 2.5% normal donkey serum in PBS for 30 min, the cells were treated with antibodies against Ki67 (Cell Signaling Technologies), phosphorylated histone H3 (pH3, Invitrogen), alpha-smooth muscle actin (Acta2, Invitrogen), GFP (Invitrogen), and alpha-actinin (Abcam) overnight at 4 °C. The cells were then incubated with Alexa Fluor 555, 488, or 350 (Invitrogen) secondary antibodies for 1 h in the dark at 37 °C.

Regarding immunostaining *in vivo*, heart sections were first incubated with 2.5% normal donkey serum in PBS for 30 min at room temperature and then treated with antibodies against Ki67 (Invitrogen), pH3 (Invitrogen), GFP (Invitrogen), Yap (Invitrogen), and cardiac troponin I (CTnI, Abcam) overnight at 4 °C. The sections were then washed thrice with PBS and incubated with Alexa Fluor 555, 488, or 350 (Invitrogen) secondary antibodies for 1 h in the dark at 37 °C.

To detect F-actin and G-actin, Alexa Fluor Plus 647 Phalloidin (Invitrogen) and Alexa Fluor 488 DNase I (Invitrogen) were utilized, respectively. For the EdU (5-ethynyl-2′-deoxyuridine, Thermo Fisher Scientific) pulse-chase experiment *in vivo*, the animals were intraperitoneally injected with 500 μg of EdU per animal every two days. EdU was visualized using a Click-iT Plus EdU Alexa Fluor 555 Imaging Kit (Invitrogen), according to the manufacturer's instructions. TUNEL (TdT-mediated dUTP Nick-End Labeling) staining was performed using a One Step TUNEL Apoptosis Assay Kit (Beyotime Biotechnology), according to the manufacturer's instructions. The nuclei were labelled with DAPI (Solarbio). The images were captured using an Olympus confocal laser scanning microscope (FluoView 3000, Japan), and areas of interest were analyzed using the Fiji software.

2.10. Measurement of cardiomyocyte size and roundness

The size of cardiomyocytes was measured using wheat germ agglutinin (WGA) staining (Invitrogen). First, the heart sections were treated with an antibody against CTnI (Abcam) overnight at 4 °C. Subsequently, the sections were washed with PBS three times and incubated with Alexa Fluor 555 (Invitrogen) secondary antibody for 1 h in the dark at 37 °C. Finally, following the manufacturer's instructions, Alexa Fluor 488-conjugated WGA was added to the heart sections. The roundness of cardiomyocytes was measured using the least squares circle method[10]. Specifically, concentric inscribed and circumscribed circles were drawn on the outline of cardiomyocytes as revealed by WGA staining, and the roundness error was calculated as the radius difference between the two circles ($\Delta R = R_{max} - R_{min}$)[10].

2.11. Quantitative real-time polymerase chain reaction (qPCR)

Total RNA was isolated from hearts using Trizol reagent (Takara), according to the manufacturer's protocols. One μg of RNA per sample was reversely transcribed into cDNA using PrimeScript RT Master Mix (Takara) with random primers. Three duplicates with cDNA and TB Green® Premix Ex Taq (Takara) were performed in CFX96 Real-Time PCR Detection System (Bio-RAD, USA). PCR was conducted in a 10 μL reaction system. Reverse transcription was performed at 37 °C for 15 min, and cDNA was amplified for 39 cycles: 95 °C for 10 s, 58 °C for 20 s, and 72 °C for 10 s. The values were normalized to *Gapdh* to calculate the relative RNA expression levels. The primer sequences used to detect mRNA expression are listed in Table S1.

2.12. Western blot analysis

For Western blotting, the total proteins of samples were isolated by normal RIPA lysis buffer, and the protein samples were prepared with a 5 × sample loading buffer and resolved by SDS-PAGE. The proteins transferred onto nitrocellulose membranes were probed with antibodies against Dystrophin (Proteintech), Thymosin beta 10 (Invitrogen), Thymosin beta 4 (Proteintech), Catenin alpha 3 (Proteintech), and GAPDH (Proteintech). For isolation of G-actin and F-actin, the G-actin/F-actin In Vivo Assay Kit (Cytoskeleton) was used according to the manufacturer's instructions. The chemiluminescent signals were detected by LiCor Odyssey Fc instrument.

2.13. Aurkb-rox-RFP/Tnnt2-Dre transgenic mice

The *Aurkb*-rox-RFP and *Tnnt2*-Dre knock-in mouse lines used in this study have been previously described[11]. To induce MI in neonatal mice, the LAD coronary artery was ligated at 1 day of age[2]. Anesthesia was induced by hypothermia on an ice bed, followed by a thoracotomy at the fourth intercostal region. The origin of the LAD coronary artery was then sutured with 7-0 silk. To induce MI in adult mice, the LAD was ligated at 8 weeks of age[2]. Tnnt2-2D2P-NIL or Control-NIL viruses were intramyocardially injected 7 days after MI. The hearts were collected for histological analysis at 14 and 21 days after MI.

2.14. Mosaic analysis with double markers (MADM) transgenic mice

$MADM^{GT/TG}$ and α-MHC-MerCreMer were purchased from the Jackson Laboratory. The Tnnt2-2D2P-NIL or Control-NIL viruses were intramyocardially injected 7 days after MI. Tamoxifen (Sigma−Aldrich) dissolved in corn oil was injected intraperitoneally into mice at the dose of 40 mg/kg on 9, 11, and 13 days after MI. The hearts were harvested for histological analysis 14 days after MI. After the nuclei of heart cryosections were labeled with DAPI (Solabio), the images were captured using an Olympus VS200 Research Slide Scanner (Japan). The percentage of single-colored cardiomyocytes from the total labeled cardiomyocytes was analyzed.

2.15. snRNA-seq data processing

The counts matrices were downloaded from the GEO database (GSE 130699, https://www.ncbi.nlm.nih.gov/geo/query/acc.cgi?acc=GSE130699), which were conducted on pericentriolar material 1-positive ($PCM1^+$) cardiomyocyte nuclei of regenerated hearts 1 and 3 days after surgery-induced MI on postnatal Day 1[6]. SnRNA-seq library preparation and sequencing were performed as described previously[6] with optimizations for the heart tissues after treatment with Tnnt2-2D2P-NIL or Control-NIL viruses. The data were deposited in the GEO database under accession number GSE246250 (https://www.ncbi.nlm.nih.

gov/geo/query/acc.cgi?acc=GSE246250). R package Seurat (v.4.0.1) was used to integrate each snRNA-seq dataset, visualize uniform manifold approximation projection (UMAP) algorithm, and score cell cycle index[12]. The removal of batch effects was processed in R using the package Harmony (v.0.1.0)[13]. For pseudotime trajectory analysis, the dimensionality reduction results were reformatted for compatibility with the learn-graph function in the R package MONOCLE3 (v.1.0.0)[14].

2.16. Statistical analysis

Software GraphPad Prism 9.0 was used to conduct statistical analyses. In our experiments, the mean and standard error were selected to represent all numerical data. To check for normality, the Shapiro−Wilk test was used. Depending on the homogeneity of variance, a two-tailed unpaired Student's *t*-test was performed to compare two groups of normally distributed data with or without Welch's correction. When homogeneity of variance was assumed, statistical analyses for comparisons of more than two groups were conducted using one-way ANOVA; otherwise, Brown−Forsythe and Welch ANOVA tests with Dunnett's T3 multiple comparisons were utilized. Two-way ANOVA was used when there were two factors. Multiple *t*-tests were used to analyze numeric data at different time points. The F-test was used to detect differences in data distribution. Results are considered statistically significant if their *P*-values are less than 0.05.

3. Results

3.1. Single-nucleus RNA sequencing analysis reveals that actin cytoskeletal remodeling contributes to dedifferentiation, proliferation, and redifferentiation of cardiomyocytes after MI

After downloading from the GEO database (GSE 130699), we analyzed the data on snRNA-seq of $PCM1^+$ cardiomyocyte nuclei from regenerated hearts 1 and 3 days after surgery-induced MI at postnatal day (P) 1 (Fig. 1A)[6]. The cells were clustered based on the integrated snRNA-seq data from four samples after batch correction using the Harmony algorithm (Supporting Information Fig. S1A), which led to the identification of 11 clusters of cardiomyocytes through UMAP (Fig. 1B). The cardiomyocyte-specific markers, such as *Tnnt2*, *Actc1,* and *Pcm1*, were used to identify cardiomyocytes. Proliferating cardiomyocytes, identified as CM6 cells, had increased expression of cell cycle genes, including *Mki67*, *Anln*, *Top2a*, and *Cenpe* (Fig. 1C and Fig. S1B).

Comparing the cell heterogeneity at the corresponding time after MI or sham surgery showed that the percentage of CM2 and CM3 cells was markedly increased, indicating their necessity in the acute regenerative response trajectory (Fig. 1D). The single-cell trajectory construction method utilized in this study was based on the UMAP algorithm, which enabled the identification of a cell population forming a circular trajectory of regeneration[14], including CM0, CM2, CM3, CM6, and CM8. To validate the directionality of the circular trajectory, cell-cycle scoring and regression analyses were performed, which revealed a clockwise direction corresponding to the cell cycle phases (G0/G1, S, G2/M). The pseudotime trajectory of the regenerative process was then predicted using the MONOCLE 3 algorithm (Fig. 1E and F). The circular trajectory reflected the entire process of dedifferentiation, proliferation, and redifferentiation, as indicated by the sinusoidal expression of immature (*Actc1*, *Myh7*, and *Tnni1*) and mature (*Cacna1c*, *Myh6*, and *Ryr2*) genes (Fig. 1G and H). Enrichment analysis revealed that trajectory genes were associated with oxidative phosphorylation, regulation of heart contraction, mitotic cell cycle, regulation of actin filament-based movement, cell cycle process, actomyosin structure organization, and response to oxidative stress (Fig. 1I and Supporting Information Table S2).

Previous studies have shown that disorganized sarcomeric structures are characteristics of dedifferentiated cardiomyocytes[5,15]. Our results found that changes in actin depolymerization (*Pfn1*, *Tmsb10*, and *Tmsb4x*) and polymerization (*Ctnna3*, *Dmd*, *Palld*, *Ank2*, and *Fhod3*) genes preceded the changes in cell cycle (*Cdca2*, *Ect2*, and *Top2a*) and dedifferentiated (*Acta2*) genes, and there were no changes in the expression of sarcomere organization genes (*Cav3* and *Edn1*), suggesting that actin cytoskeletal remodeling may be the fundamental driver of the change in sarcomeric structures and contributor to the dedifferentiation, proliferation, and redifferentiation of cardiomyocytes (Fig. 1J). Actin depolymerization was proven by the transformation from filamentous actin (F-actin) to globular actin (G-actin)[16], and we found that organized sarcomeres were accompanied by organized F-actin and absent G-actin, and disorganized sarcomeres were accompanied by disorganized F-actin and enriched G-actin (Fig. 1K). The percentage of disorganized F-actin was calculated by dividing the G-actin/disorganized area by the total cell area (Supporting Information Fig. S2). Additional experiments revealed that the higher percentage of disorganized F-actin correlated with the higher percentages of Ki67-, pH3-, and Acta2-positive cardiomyocytes, and G-actin intensity, suggesting that the degree of actin cytoskeletal remodeling correlated with proliferation and dedifferentiation of cardiomyocytes (Fig. 1L).

Dmd (dystrophin), a component of the dystrophin-associated glycoprotein complex, controlled actin polymerization[17] and underwent significant change during the trajectory (Fig. 1J). To show the full cycle of actin depolymerization and polymerization, NRVMs were first transfected with siRNA-*Dmd* for 0−48 h and then transfected with saRNA-*Dmd* for 48−96 h[18]. As expected, siRNA-*Dmd* triggered cardiomyocyte differentiation, as evidenced by the remodeling from a cross-striated pattern to a highly diffuse pattern for the sarcomeric Z-line marker *Actn2* (α-actinin)[19], accompanied by the gradual increase in Ki67-positive cardiomyocytes, G-actin intensity, and percentage of disorganized F-actin. However, these changes were reversed by saRNA-*Dmd* (Fig. 1M).

Our group developed an Aurora kinase B-based mouse system to identify and analyze proliferating cardiomyocytes marked by red fluorescence protein (RFP/tdTomato) (Supporting Information Fig. S3A)[11]. We then used this system to calculate the percentage of disorganized F-actin by dividing the F-actin absent area by the cell area and discovered that in both neonatal and adult post-MI hearts, the percentage of disorganized F-actin was significantly higher in RFP-positive cardiomyocytes compared with RFP-negative cardiomyocytes (Fig. S3B and S3C). Taken together, these findings showed a continuous trajectory of cardiac regeneration from a global perspective and demonstrated that actin remodeling contributed to the dedifferentiation, proliferation, and redifferentiation of cardiomyocytes after injury, which provided a more detailed chronological substructure of cardiomyocyte renewal and advanced our understanding of actin cytoskeletal organization at a single-cell resolution across this progression.

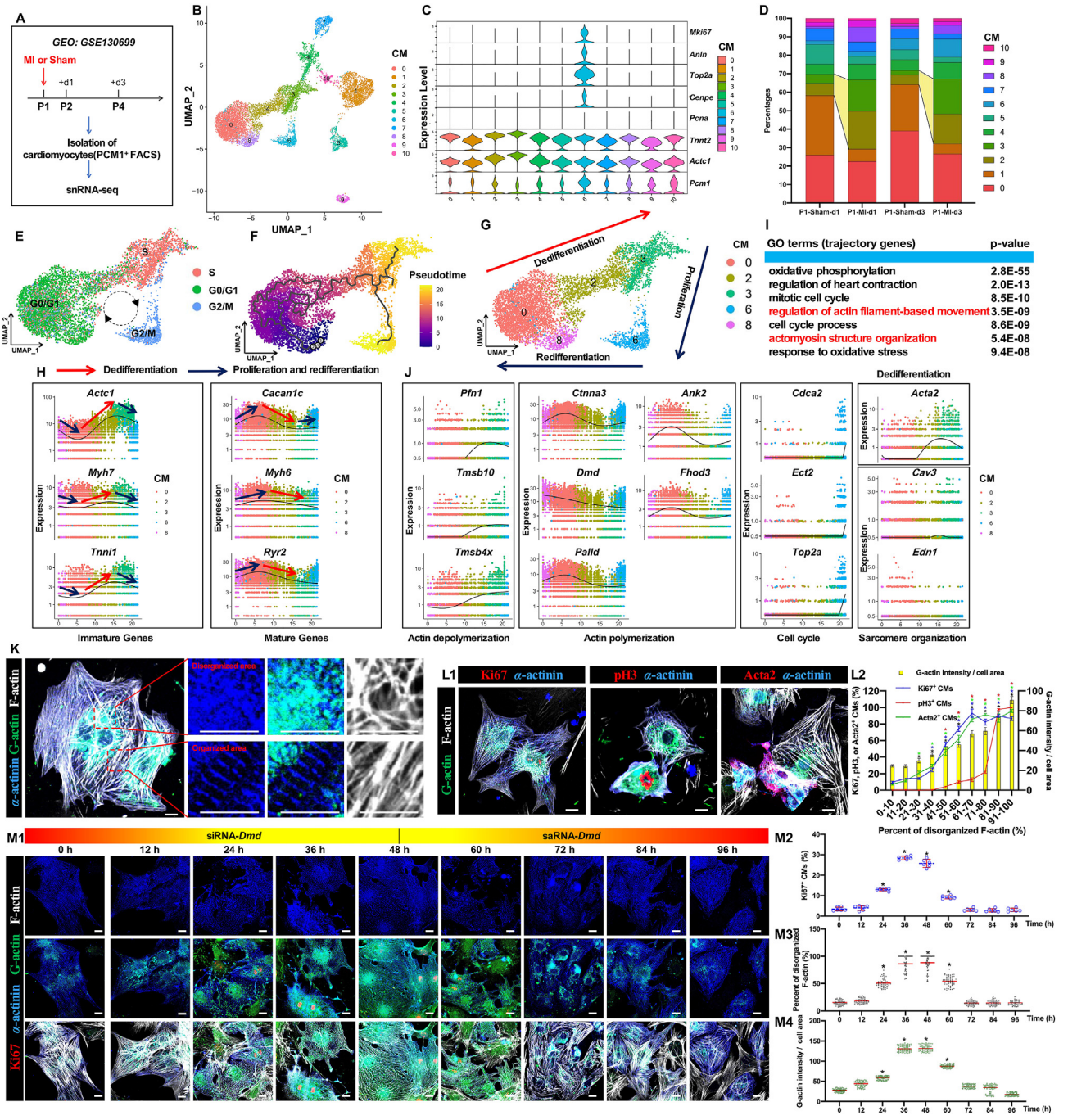

Figure 1 Single-nucleus RNA sequencing analysis reveals that actin cytoskeletal remodeling contributes to the dedifferentiation, proliferation, and redifferentiation of cardiomyocytes after myocardial infarction. (A) Schematic diagram showing the experimental design for snRNA-seq analysis; sequencing was performed in isolated nuclei from hearts on postnatal Days 1 and 3 after surgery-induced myocardial infarction or sham. (B) Uniform manifold approximation projection (UMAP) visualization of different cardiomyocyte clusters. (C) Violin plots showing the expression of cardiomyocyte-specific genes (*Tnnt2, Actc1,* and *Pcm1*) and proliferating genes (*Mki67*, *Anln*, *Top2a*, *Cenpe,* and *Pcna*). (D) Fraction of cardiomyocyte populations in each snRNA-seq sample. (E) The cell cycle analysis in CM0, CM2, CM3, CM6, and CM8 cells. (F) Pseudotime analysis revealed a circular trajectory of CM0, CM2, CM3, CM6, and CM8 cells. (G) UMAP visualization of cardiomyocyte clusters in the circular trajectory revealed the regenerative processes of dedifferentiation, proliferation, and redifferentiation. (H) Pseudotime analysis revealed the sinusoidal expression of immature (*Actc1*, *Myh7*, and *Tnni1*), and mature (*Cacna1c*, *Myh6*, and *Ryr2*) genes. (I) Top GO terms for trajectory genes in CM0, CM2, CM3, CM6, and CM8 cells. (J) Pseudotime analysis revealed the expression curves of actin depolymerization (*Pfn1*, *Tmsb10*, and *Tmsb4x*), actin polymerization (*Ctnna3*, *Dmd*, *Palld*, *Ank2*, and *Fhod3*), cell cycle (*Cdca2*, *Ect2*, and *Top2a*), dedifferentiation (*Acta2*), and sarcomere organization (*Cav3*, and *Edn1*) genes. (K) F-actin (white), G-actin (green), and α-actinin (blue) staining of neonatal rat ventricular myocytes (NRVMs) showing the organized and disorganized actin cytoskeleton. Scale bar, 10 μm. (L) Staining of F-actin (white), G-actin (green), α-actinin (blue), Ki67 (red), pH3 (red), and Acta2 (red) in NRVMs (L1). Scale bar, 10 μm. Quantification of G-actin intensity and

3.2. *Transient transfection of the 2D2P genes using a non-integrating lentivirus system induced transient actin remodeling and a transient increase in cardiomyocyte proliferation* in vitro

To determine the critical factors of actin remodeling that influenced cardiomyocyte proliferation, we examined all actin remodeling genes involved in the trajectory of cardiac regeneration, including polymerization genes (*Dmd*, *Ctnna3*, *Palld*, *Ank2*, *Fhod3*, and *Diaph3*) and depolymerization genes (*Tmsb4x*, *Tmsb10*, *Pfn1*, and *Cfl1*). The expression patterns of these genes were analyzed, and we found that the changes in polymerization genes were down-regulated and then up-regulated, whereas the changes in depolymerization genes were up-regulated and then down-regulated (Fig. 2A). We then ranked the genes based on their maximum variation of expression (ΔExpression) (Fig. 2B, Supporting Information Fig. S4A). Subsequently, we silenced each of the 11 genes in purified primary cardiomyocytes harvested from postnatal Day 7 mice, when most cardiomyocytes had become post-mitotic[20,21]. After 48 h of transfection, we observed that silencing of *Dmd*, *Ctnna3*, *Tmsb4x*, and *Tmsb10* individually influenced the percentage of pH3-positive cardiomyocytes, which were the top two depolymerization (2D) and polymerization (2P) genes (Fig. 2C). The separate level changes of 2D2P genes were inconspicuous in the average of each sample (Fig. S4B), but there were conspicuous changes of 2D2P genes in different clusters of the regenerative trajectory (Fig. S4C). Based on the synchronous and sinusoidal changes of 2D2P genes, which drove the complete process of dedifferentiation, proliferation, and redifferentiation in cardiomyocytes, we developed a strategy for 2D2P delivery to transiently up-regulate the expression of 2D genes and transiently down-regulate the expression of 2P genes, using a NIL. The NIL is characterized by high infection efficiency and transient expression of target genes, whose peak lasts only 2−3 days[22-24]. This rapid degradation kinetics makes NIL an ideal gene therapy to treat various diseases in several ongoing clinical trials and an optimal delivery vehicle for the 2D2P treatment in our study[25]. Therefore, we cloned overexpressed 2D genes (*Tmsb4x*, *Tmsb10*) and silenced 2P genes (sh*Dmd*, sh*Ctnna3*) in a polycistronic lentivirus backbone, with each factor driven by a *Tnnt2* (cardiac-specific troponin T) promoter (Tnnt2-2D2P-NIL, Fig. 2D)[26]. First, we assessed the infection efficiency of Control-NIL and Tnnt2-2D2P-NIL, which were both ∼90% after 4 days and ∼10% after 8 days, as assessed by GFP immunofluorescence (Fig. 2E). We then assessed the protein expression of each 2D2P factor in postnatal Day 7 cardiomyocytes using Western blot, and the results revealed that Tnnt2-2D2P-NIL significantly induced lower protein expression of Dystrophin and Catenin α3, and higher protein expression of Thymosin β4 and β10 at 4 days after infection, which were disabled at 8 days after infection (Supporting Information Fig. S5A−S5E). Furthermore, Tnnt2-2D2P-NIL infection significantly increased the percentage of Ki67-, pH3-, and EdU-positive cardiomyocytes at 4 days after infection compared with Contol-NIL. Moreover, Tnnt2-2D2P-NIL infection induced significant disorganization of F-actin and an increase in G-actin intensity at 4 days. However, after 8 days of infection, the increase in EdU labeling persisted, but the increase in Ki67 and pH3 labelings, disorganized F-actin, and G-actin intensity decreased to the control level on day 8 (Fig. 2F−J). Furthermore, Tnnt2-2D2P-NIL significantly decreased F-actin expression and increased G-actin expression at 4 days, but these effects returned to the control level on day 8 (Supporting Information Fig. S6A−S6C), indicating that the transient transfection of 2D2P genes induced transient actin remodeling and a transient increase in cardiomyocyte proliferation.

3.3. *Transient transfection of the 2D2P genes using Tnnt2-2D2P-NIL can improve cardiac function and reduce the scar size of MI by promoting cardiomyocyte proliferation in mice*

To investigate the potential ability of Tnnt2-2D2P-NIL in promoting adult cardiac regeneration *in vivo*, we conducted experiments in 8-week-old mice with permanent ligation of the LAD. Intramyocardial injection of Tnnt2-2D2P-NIL or Control-NIL virus was performed 7 days after MI, and the changes in 2D2P expression were measured at 7 (14 days post-MI) and 14 days (21 days post-MI) after injection (Fig. 3A). The infection by Control-NIL and Tnnt2-2D2P-NIL was confirmed by GFP immunofluorescence 7 days after injection (Supporting Information Fig. S7A). Tnnt2-2D2P-NIL significantly induced lower protein expression of Dystrophin and Catenin α3, and higher protein expression of Thymosin β4 and β10 at 7 days after injection, but GFP labeling and protein expression recovered to control level at 14 days after injection (Fig. S7A−S7B). RNA expression of the silenced *Dmd*, silenced *Ctnna3*, overexpressed *Tmsb4x*, or overexpressed *Tmsb10* was only detected in the heart and not in the other organs 7 days after viral injection (Fig. S7C).

To determine the effects of Tnnt2-2D2P-NIL on cardiac function after MI *in vivo*, we performed echocardiographic analysis at the age of 8 weeks as a baseline and on 1 day, 7 days, 14 days, 21 days, and 28 days after MI (Fig. 3A). Consistent with previous reports[2,5], MI decreased cardiac function, as evidenced by decreased EF and FS, and increased LVIDd and LVIDs. The impairment in cardiac function caused by MI was significantly mitigated in the Tnnt2-2D2P-NIL group compared with the Control-NIL group 21 and 28 days after MI (Fig. 3B−E). To avoid inappropriate comparisons of absolute EF and FS values between groups due to the different baseline values 7 days after MI, we also compared the changes of EF and FS in each animal 7 and 28 days after MI (ΔEF and ΔFS). This assessment showed a significant improvement of ΔEF and ΔFS in the Tnnt2-2D2P-NIL-treated group compared with the Control-NIL group (Fig. 3F and G). Consistent with the improvement in cardiac function, infarct sizes were significantly decreased at 28 days post-MI in the Tnnt2-2D2P-NIL group (Fig. 3H).

Moreover, Tnnt2-2D2P-NIL injection significantly increased cardiomyocyte proliferation at 14 days post-MI, as indicated by increased Ki67-, pH3-, and EdU-positive cardiomyocytes both in the infarct border zone and remote zone (Fig. 3I and J). Furthermore, isolated cardiomyocyte numbers were significantly increased in the Tnnt2-2D2P-NIL-treated mice compared with

the percentage of $Ki67^+$, $pH3^+$, and $Acta2^+$ cardiomyocytes in different percentages of disorganized F-actin. $^*P < 0.05$ *vs*. 0−10. 500−600 cells in each analysis (L2). (M) Staining of F-actin (white), G-actin (green), α-actinin (blue), and Ki67 (red) in NRVMs with siRNA-*Dmd* for 48 h and saRNA-*Dmd* after 48 h (M1). Scale bar, 10 μm. Quantification of $Ki67^+$ cardiomyocytes (M2), disorganized F-actin percentage (M3), and G-actin intensity (M4) in NRVMs with siRNA-*Dmd* for 48 h and saRNA-*Dmd* after 48 h $^*P < 0.05$ *vs*. 0 h. 6 repeats/∼600 cells in each group of Ki67 quantification. 50−70 cells in each group of F-actin/G-actin quantification.

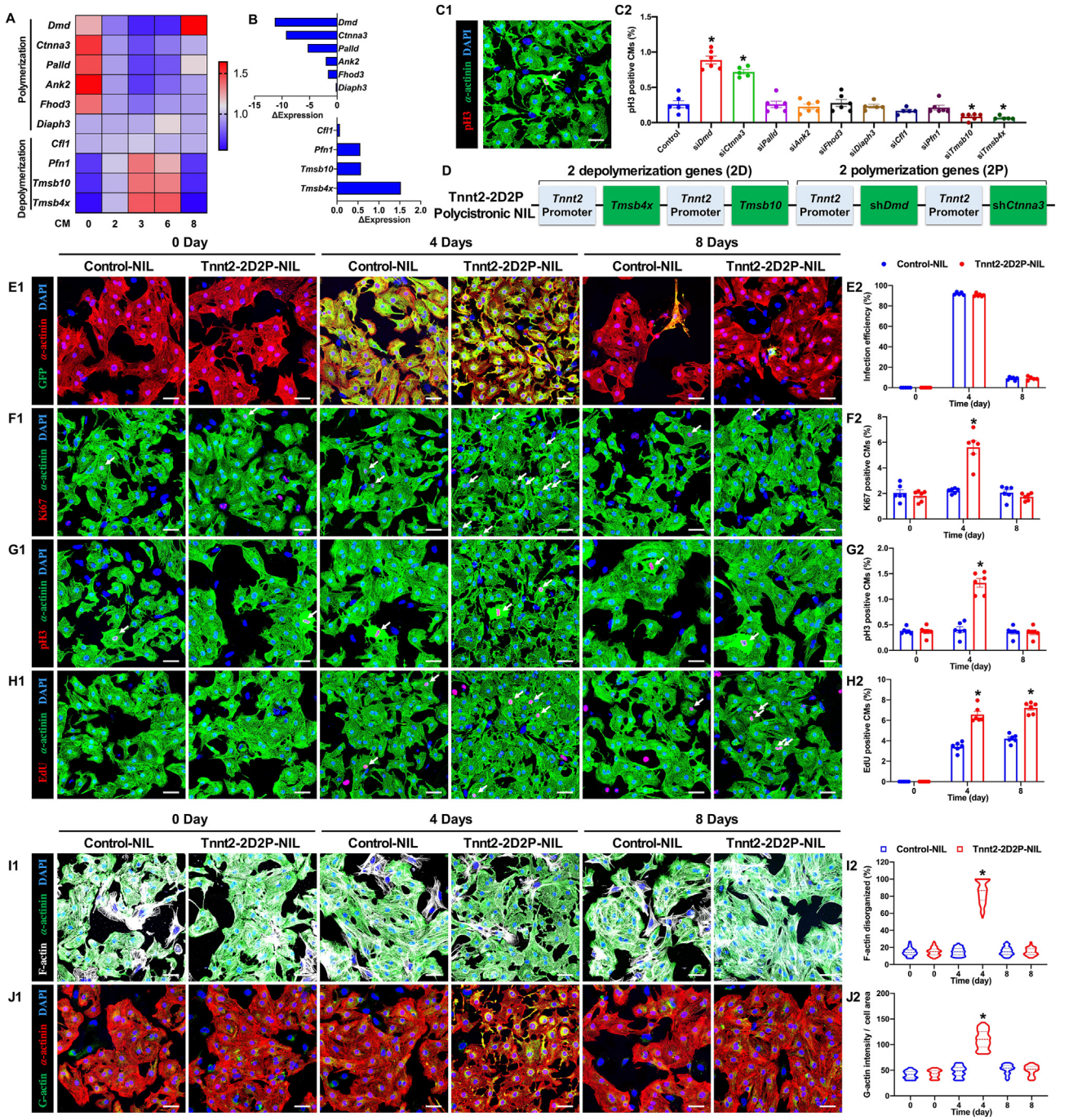

Figure 2 Transient transfection of the 2D2P genes using a non-integrating lentivirus system induces transient actin remodeling and a transient increase in cardiomyocyte proliferation *in vitro*. (A) Heatmap showing the expression patterns of actin polymerization genes (*Dmd*, *Ctnna3*, *Palld*, *Ank2*, *Fhod3*, and *Diaph3*) and actin depolymerization genes (*Cfl1*, *Pfn1*, *Tmsb10*, and *Tmsb4x*) in CM0, CM2, CM3, CM6, and CM8 cells. (B) The ranking of maximum variation of expression (ΔExpression) in actin polymerization (*Dmd*, *Ctnna3*, *Palld*, *Ank2*, *Fhod3*, and *Diaph3*) and depolymerization (*Cfl1*, *Pfn1*, *Tmsb10*, and *Tmsb4x*) genes. (C) Staining of DAPI (blue), pH3 (red), and α-actinin (green) in neonatal mouse ventricular myocytes (NMVMs) from postnatal Day 7 (P7) mice (C1). Scale bar, 20 μm. Quantification of $pH3^+$ cardiomyocytes in NMVMs from P7 mice treated with siRNA for 48 h. $*P < 0.05$ *vs*. Control. 6 repeats/∼600 cells in each group (C2). (D) Schematic diagram of the plasmid design for Tnnt2-2D2P polycistronic NIL. (E−H) Representative images of NMVMs from postnatal Day 7 mice treated with Control-NIL or Tnnt2-2D2P-NIL for 0, 4, or 8 days and immunostained for DAPI (blue), GFP (green), Ki67 (red), pH3 (red), EdU (red), and α-actinin (red/green) (E1−H1). Scale bar, 20 μm. Quantification of GFP^+ (E2), $Ki67^+$ (F2), $pH3^+$ (G2), and EdU^+ (H2) cardiomyocytes. $*P < 0.05$ *vs*. Control-NIL. 5−6 repeats/400−600 cells in each group. (I, J) Representative images of NMVMs from postnatal Day 7 mice treated with Control-NIL or Tnnt2-2D2P-NIL for 0, 4, or 8 days and immunostained for DAPI (blue), F-actin (white), G-actin (green), and α-actinin (green/red) (I1−J1). Scale bar, 20 μm. Quantification of disorganized F-actin percentage (I2), and G-actin intensity (J2) in cardiomyocytes. $*P < 0.05$ *vs*. Control-NIL. 100−120 cells in each group.

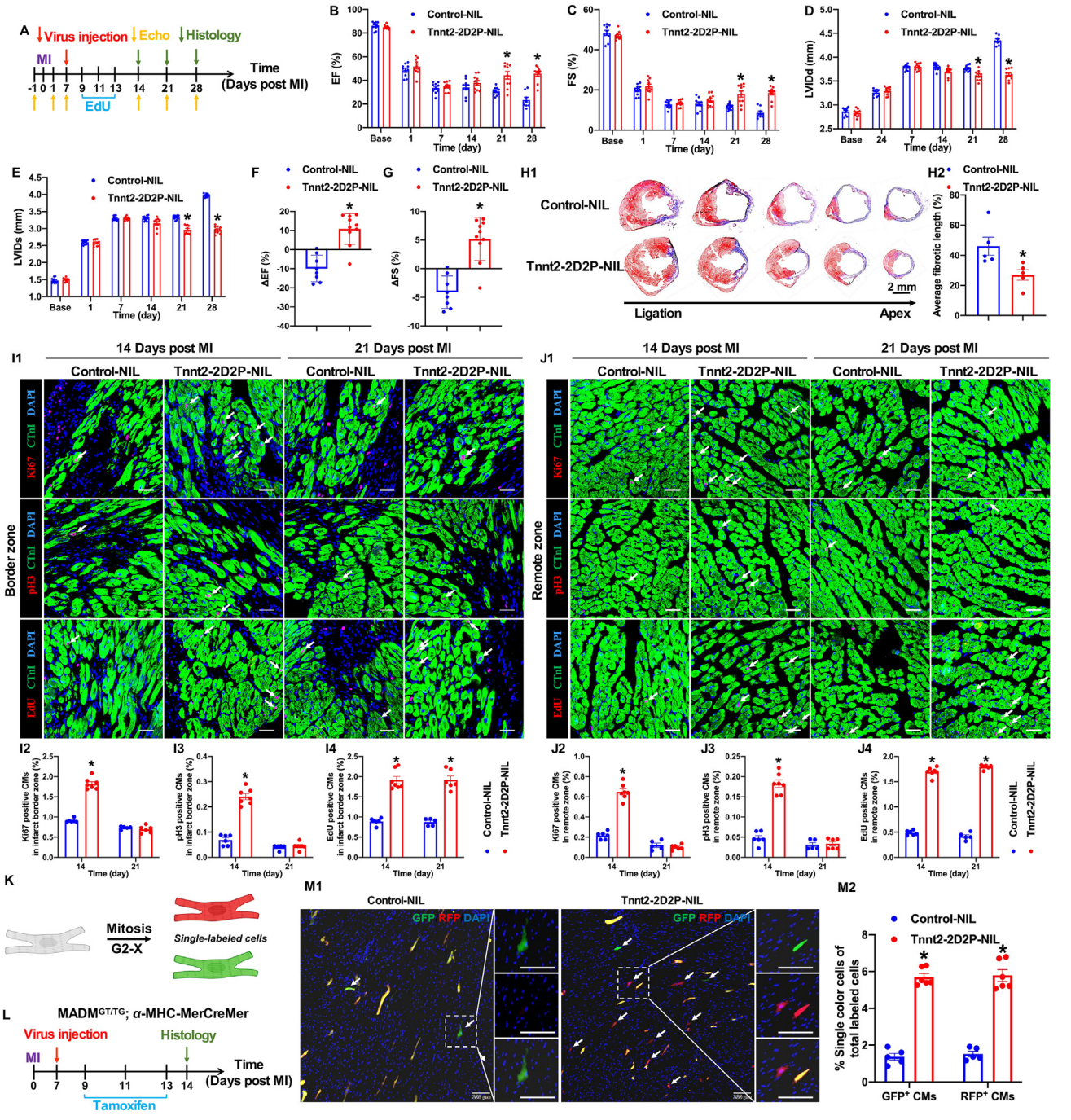

Figure 3 Transient transfection of the 2D2P genes using Tnnt2-2D2P-NIL can improve cardiac function and reduce scar size after myocardial infarction by promoting cardiomyocyte proliferation in mice. (A) Schematic diagram of the experimental design for virus injection of Control-NIL or Tnnt2-2D2P-NIL in mice with myocardial infarction (MI). Echocardiographic analysis was performed at the age of 8 weeks as a baseline and 24 h, 7, 14, 21, and 28 days after MI. Intramyocardial injection of Tnnt2-2D2P-NIL or Control-NIL virus was performed 7 days after MI. EdU was intraperitoneally injected on 9, 11, and 13 days after MI. (B−E) Quantification of left ventricular ejection fraction (EF%, B), fraction shortening (FS%, C), left ventricular internal diastolic diameter (LVIDd, D), and left ventricular internal systolic diameter (LVIDs, E). $n = 8-10$. $^*P < 0.05$ *vs.* Control-NIL. (F, G) Quantification of the change in EF% (ΔEF%, F) and FS% (ΔFS%, G) for each mouse between 7 and 28 days after MI. $n = 8-10$. $^*P < 0.05$ *vs.* Control-NIL. (H) Serial sectioning was performed at 500 μm intervals from the ligation area to the apex. Representative images (H1) and quantification (H2) of infarct length by Masson's trichrome staining 28 days after MI. Scale bar, 2 mm. $n = 5$. $^*P < 0.05$ *vs.* Control-NIL. (I, J) Representative images (I1, J1) and quantification (I2, I3, I4, J2, J3, and J4) of $Ki67^+$, $pH3^+$, and EdU^+ cardiomyocytes of Control-NIL or Tnnt2-2D2P-NIL treated hearts in infarct border and remote zones at 14 or 21 days after MI. Scale bar, 20 μm. $n = 5-7$. $^*P < 0.05$ *vs.* Control-NIL. (K) Mosaic analysis with double markers (MADM) recombination in a parent cardiomyocyte in α-MHC-expressing cells leads to RFP^+ and GFP^+ single-labeled daughter cardiomyocytes. (L) Schematic diagram of the experimental design for the injection with Control-NIL or Tnnt2-2D2P-NIL in MADM mice. Tamoxifen was intraperitoneally injected at 9, 11, and 13 days after MI. (M) Representative images (MI) and quantification (M2) of the percentage of single-colored cells to total labeled cells in MADM mouse hearts treated with Control-NIL or Tnnt2-2D2P-NIL. Scale bar, 100 μm. $n = 5-6$. $^*P < 0.05$ *vs.* Control-NIL.

Control-NIL-treated mice (Supporting Information Fig. S8A). However, at 21 days post-MI, although the increase in cardiomyocyte number and EdU labeling persisted, the increase in Ki67 and pH3 labeling had returned to the control level, indicating a transient cardiomyocyte expansion induced by Tnnt2-2D2P-NIL (Fig. 3I and J, Fig. S8A). To confirm the efficacy of Tnnt2-2D2P-NIL in promoting authentic cytokinesis of cardiomyocytes, we used two cardiomyocyte cytokinesis animal models. One was the inducible cardiomyocyte cytokinesis lineage-tracing mice ($MADM^{GT/TG}$:α-MHC-MerCreMer), in which single-colored green (GFP^+) or red (RFP^+) cardiomyocytes had definitively undergone completed cytokinesis (Fig. 3K)[27]. MADM mice at 8 weeks old were subjected to MI, and Tnnt2-2D2P-NIL or Control-NIL was injected intramyocardially 7 days after MI. Tamoxifen was injected at 9, 11, and 13 days after MI to stimulate recombination events (Fig. 3L). Fourteen days after MI, the hearts of Tnnt2-2D2P-NIL-treated MADM mice showed a significant increase in the proportion of both RFP^+ and GFP^+ cardiomyocytes (Fig. 3M, Supporting Information Fig. S9). Another model was the *Aurkb*-rox-RFP/*Tnnt2*-Dre mice, in which *Aurkb* (a cytokinesis marker) expression was labeled with RFP (tdTomato)[11]. Tnnt2-2D2P-NIL injection also significantly increased RFP^+ cardiomyocytes at 14 days post-MI, and this increase was no longer observed at 21 days post-MI (Supporting Information Fig. S10A).

To profile the regenerative effect of Tnnt2-2D2P-NIL treatment at single-cell resolution, we performed snRNA-seq on post-MI hearts 7 days after virus injection (Fig. 4A). We assigned a total of 22,928 nuclei (10,291 nuclei from Control-NIL group and 12,637 nuclei from Tnnt2-2D2P-NIL group) into 6 distinct clusters, which were visualized by UMAP (Fig. 4B) after batch correction (Fig. 4C). Based on cell type-specific markers (Fig. 4D), we identified the major cardiac cell types, including cardiomyocytes (*Tnnt2*, *Actc1*, *Pcm1*), fibroblasts (*Postn*, *Fbn1*, *Col5a1*), endothelial cells (*Pecam1*, *Flt1*, *Tie1*), smooth muscle cells (*Pdgfrb*, *Notch3*, *Cspg4*), epicardium cells (*Wt1*, *Upk3b*, *Muc16*), and blood cells (*Mrc1*, *Fyb*, *Cd86*). Next, we clustered the subset of cardiomyocytes, which led to the identification of 5 clusters of cardiomyocytes through UMAP (Fig. 4E). Proliferating adult cardiomyocytes (ACM), identified as ACM2 cells, had increased expression of cell cycle genes, including *Mki67*, *Anln*, *Top2a*, and *Cenpe* (Fig. 4F). There was a 10-fold increase in the number of ACM2 in Tnnt2-2D2P-NIL group (7.78%, 460/5915 nuclei) compared with Control-NIL group (0.77%, 20/2602 nuclei) (Fig. 4G), and $Mki67^+$, $Anln^+$, $Top2a^+$, or $Cenpe^+$ cardiomyocytes were increased in Tnnt2-2D2P-NIL group (Fig. 4H), which was consistent with our previous immunostaining results. Taken together, our results suggested that Tnnt2-2D2P-NIL treatment induced transient cardiomyocyte expansion, which was able to improve cardiac function and reduce scar size in mice after MI.

3.4. *Transient transfection of 2D2P genes using Tnnt2-2D2P-NIL induced transient actin remodeling of cardiomyocytes in mice with MI*

Consistent with the transient increase in cardiomyocyte proliferation induced by Tnnt2-2D2P-NIL injection, this group also had a significant reduction in cardiomyocyte cross-sectional area in both the infarct border zone and remote zone at 14 days post-MI, that recovered to control levels 21 days post-MI (Fig. 5A and B). Additionally, the least squares circle method was used to assess cardiomyocyte roundness error (Supporting Information Fig. S11A−S11C)[10], and similar results were found. Tnnt2-2D2P-NIL injection significantly reduced roundness error in both the infarct border zone and remote zone at 14 days post-MI, that recovered to control levels at 21 days post-MI (Fig. 5A and B). These results suggested that Tnnt2-2D2P-NIL had a transient effect on the narrowing and rounding of cardiomyocytes, possibly due to changes in the support provided by the actin cytoskeleton network[28]. Furthermore, cardiomyocytes treated with Tnnt2-2D2P-NIL showed a broader range of distribution in orientation angles[29] compared with the Control-NIL group at 14 days post-MI, but this difference in distribution was no longer observed at 21 days post-MI (Fig. 5C, Supporting Information Fig. S12).

In myocardial tissue sections, cardiomyocytes with disorganized F-actin appeared as cavities in the cytoskeleton, which may be due to the support provided by surrounding cells (Supporting Information Fig. S13). Tnnt2-2D2P-NIL injection significantly increased the percentage of cardiomyocytes with disorganized F-actin at 14 days post-MI in both the infarct border zone and remote zone, which recovered to control levels at 21 days post-MI (Fig. 5D and E). Isolated individual cardiomyocytes with disorganized F-actin appeared to be contracted, which may be due to the loss of support from surrounding tissue cells. Based on the morphology of F-actin, isolated cardiomyocytes were classified into three categories: not disorganized, moderately disorganized, and severely disorganized (Fig. 5F). Tnnt2-2D2P-NIL injection significantly increased the percentage of moderately disorganized and severely disorganized cardiomyocytes at 14 days post-MI, but these differences were no longer observed at 21 days post-MI (Fig. 5F). Additionally, Tnnt2-2D2P-NIL significantly decreased the expression of F-actin and significantly increased the expression of G-actin at 14 days post-MI, but these effects recovered to control levels at 21 days post-MI (Fig. 5G and H). Despite changes in the actin cytoskeleton, there were no obvious ventricular arrhythmic episodes, atrial fibrillation, or fatal arrhythmia monitored at 14 days post-MI (Supporting Information Fig. S14). These data suggested that Tnnt2-2D2P-NIL treatment induced transient actin remodeling of cardiomyocytes in mice after MI.

3.5. *Tnnt2-2D2P-NIL promoted F-actin and sarcomeric disassembly through the synergistic effect of Yap nuclear translocation and G-actin sequestration*

The inactivation of both Dystrophin and Catenin α3 is related to increased Yap nuclear translocation and sarcomeric disassembly[29,30], moreover, actin dynamics and Yap signaling have a mutually regulating effect[31]. The amino acid fragment "LKKTET" of Thymosin β4 and Thymosin β10 is responsible for the initial interaction with G-actin, which sequesters G-actin and blocks F-actin polymerization[32]. To examine Yap expression after Tnnt2-2D2P-NIL treatment, we performed immunofluorescent staining with anti-Yap antibody on hearts at 14 days post-MI. The cardiomyocyte numbers of Yap-positive nuclei in the Tnnt2-2D2P-NIL treated hearts were significantly increased in both the infarct border zone and remote zone (Supporting Information Fig. S15A). In isolated adult cardiomyocytes, Control-NIL treated cardiomyocytes exhibited very low levels of Yap in nuclei, but Yap was observed at high levels in the nuclei of Tnnt2-2D2P-NIL treated cardiomyocytes (Fig. S15B). Lastly, Tnnt2-2D(Mut)2P-NIL was constructed with "LKKTET" truncated mutations in Thymosin β4 and Thymosin β10 (Supporting Information Fig. S16A−S16C), and Tnnt2-2D(Mut)2P-NIL failed to induce cardiomyocyte proliferation, F-actin and sarcomeric disassembly in the presence of Verteporfin, an inhibitor of Yap-TEAD

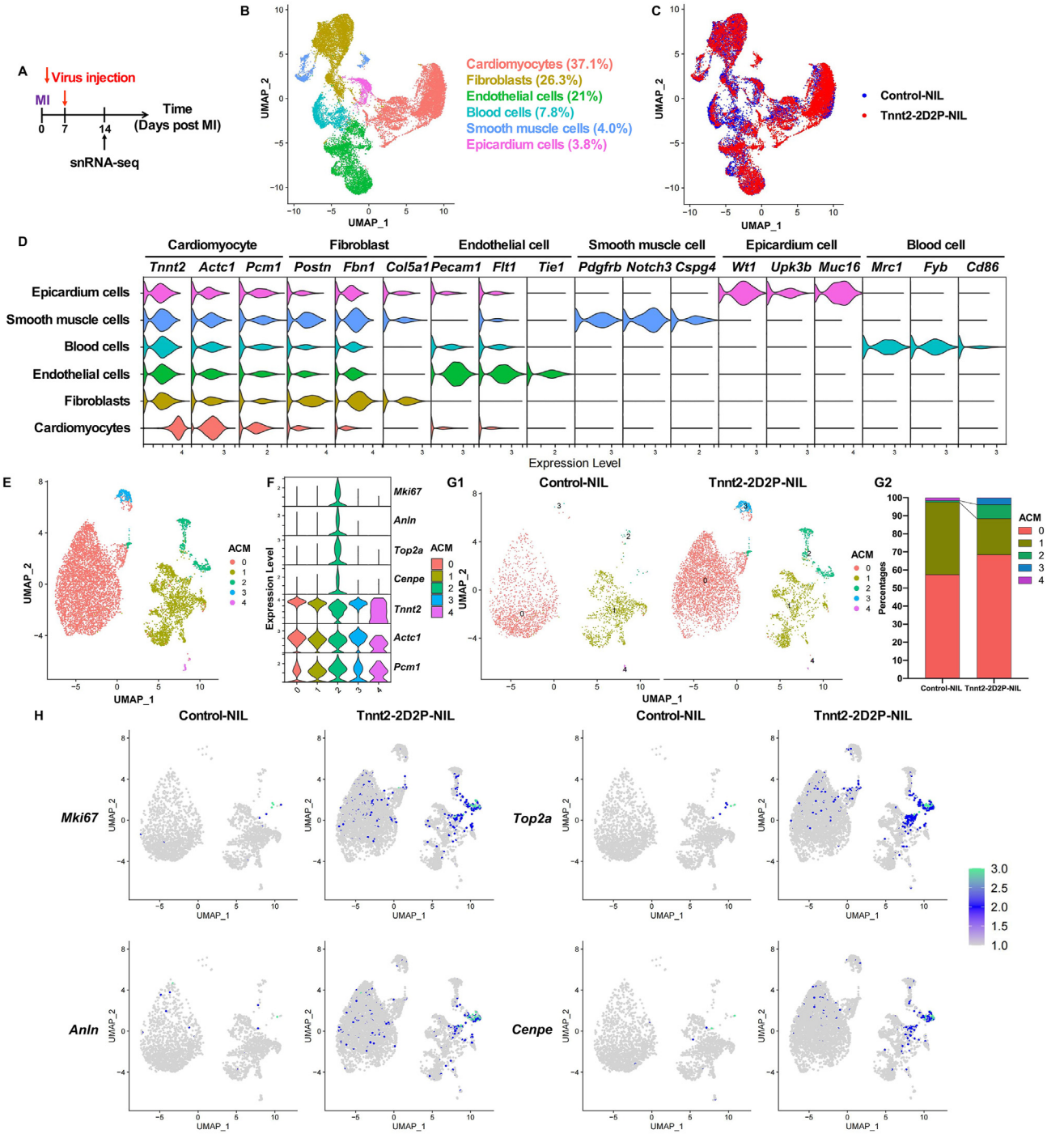

Figure 4 Single-nucleus RNA sequencing analysis reveals regenerative effect of Tnnt2-2D2P-NIL treatment. (A) Schematic diagram showing the experimental design for snRNA-seq analysis; sequencing was performed on post-MI hearts 7 days after virus injection. (B) Uniform manifold approximation projection (UMAP) visualization of different cell clusters. (C) UMAP visualization grouped by different samples. (D) Violin plots showing the expression of cell-specific genes, including cardiomyocytes (*Tnnt2*, *Actc1*, and *Pcm1*), fibroblasts (*Postn*, *Fbn1*, and *Col5a1*), endothelial cells (*Pecam1*, *Flt1*, and *Tie1*), smooth muscle cells (*Pdgfrb*, *Notch3*, and *Cspg4*), epicardium cells (*Wt1*, *Upk3b*, and *Muc16*), and blood cells (*Mrc1*, *Fyb*, and *Cd86*). (E) UMAP visualization of different cardiomyocyte clusters. (F) Violin plots showing the expression of cardiomyocyte-specific genes (*Tnnt2*, *Actc1*, and *Pcm1*) and proliferating genes (*Mki67*, *Anln*, *Top2a,* and *Cenpe*). (G) UMAP visualization grouped by different cardiomyocyte clusters and samples (G1); Fraction of cardiomyocyte populations in each snRNA-seq sample (G2). (H) Feature plots showing the expression of proliferating genes (*Mki67*, *Anln*, *Top2a,* and *Cenpe*) grouped by different samples.

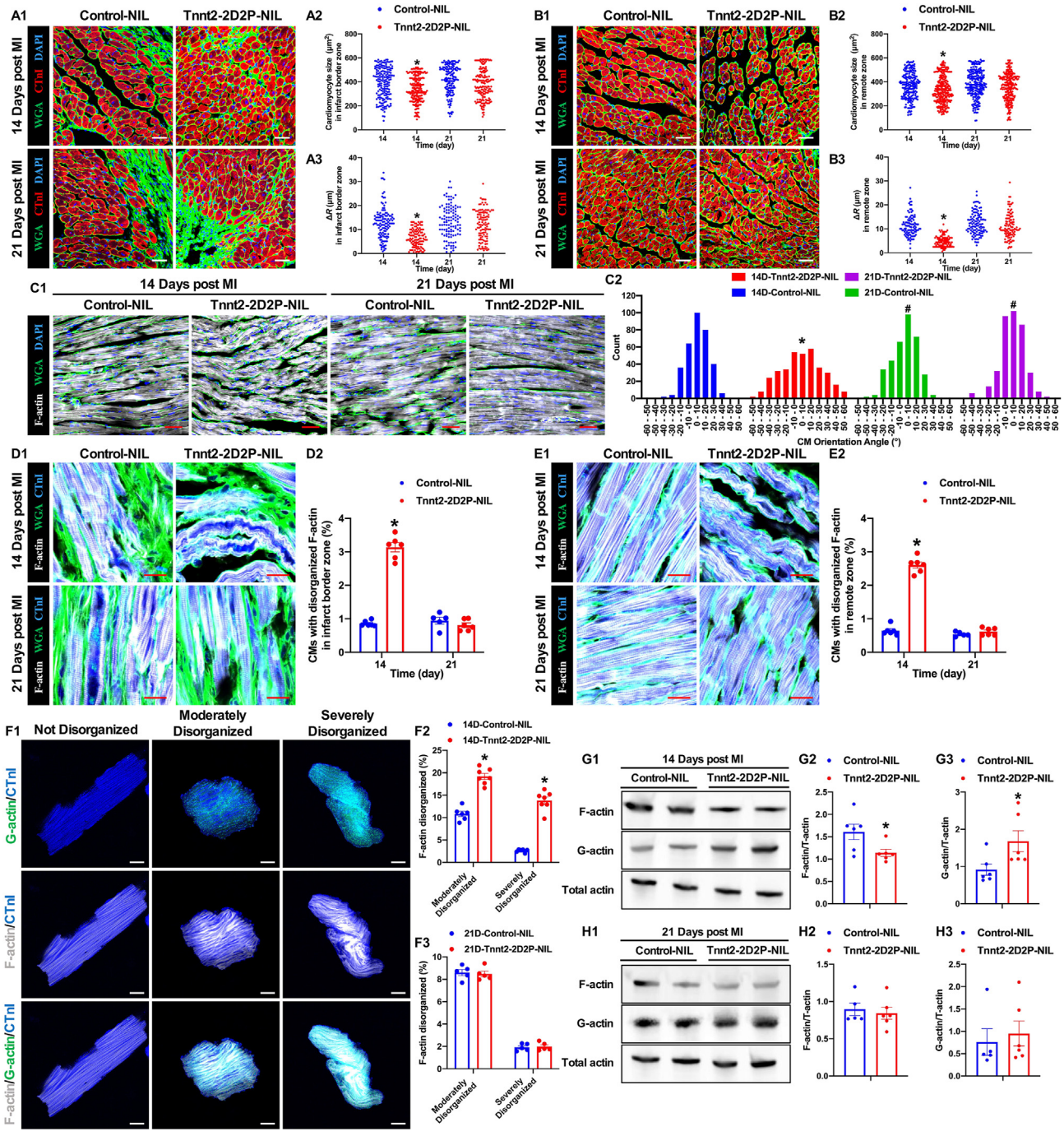

Figure 5 Transient transfection of the 2D2P genes using Tnnt2-2D2P-NIL induces transient actin remodeling of cardiomyocytes in mice after myocardial infarction. (A, B) Representative images (A1, B1) of mouse hearts at the infarct border and remote zones stained with wheat germ agglutinin (WGA, green), DAPI (blue), and CTnI (red). Scale bar, 20 μm. Quantification of cardiomyocyte size (A2, B2) and ΔR (A3, B3) of Control-NIL or Tnnt2-2D2P-NIL treated hearts in infarct border and remote zones at 14 or 21 days after myocardial infarction (MI). 150−300 cells from 5 to 7 mice for cardiomyocyte size quantification. ~120 cells from 5 to 7 mice for ΔR quantification. $^*P < 0.05$ *vs*. Control-NIL. (C) Representative images (C1) and histograms (C2) showing the distribution of cardiomyocyte orientation angles in Control-NIL or Tnnt2-2D2P-NIL treated hearts at 14 or 21 days after MI. Scale bar, 20 μm. 330−370 cells from 5 to 7 mice. $^*P < 0.05$ *vs*. 14D-Control-NIL; $^{\#}P < 0.05$ *vs*. 14D-Tnnt2-2D2P-NIL. (D, E) Representative images (D1, E1) and quantification (D2, E2) of the percentage of cardiomyocytes with disorganized F-actin in Control-NIL or Tnnt2-2D2P-NIL treated hearts in infarct border and remote zones at 14 or 21 days after MI. Scale bar, 10 μm. $n = 5$−6. $^*P < 0.05$ *vs*. Control-NIL. (F) Representative images (F1) and quantification (F2, F3) of the percentage of isolated cardiomyocytes with moderately or severely disorganized F-actin in Control-NIL or Tnnt2-2D2P-NIL treated hearts at 14 or 21 days after MI. Scale bar, 10 μm. 1300−1500 cells from 5 to 7 mice. $^*P < 0.05$ *vs*. Control-NIL. (G, H) Representative images (G1, H1) and quantification (G2, G3, H2, H3) of F-actin, G-actin, and total-actin expressions in Control-NIL or Tnnt2-2D2P-NIL treated hearts at 14 or 21 days after MI. $n = 5$−6. $^*P < 0.05$ *vs*. Control-NIL.

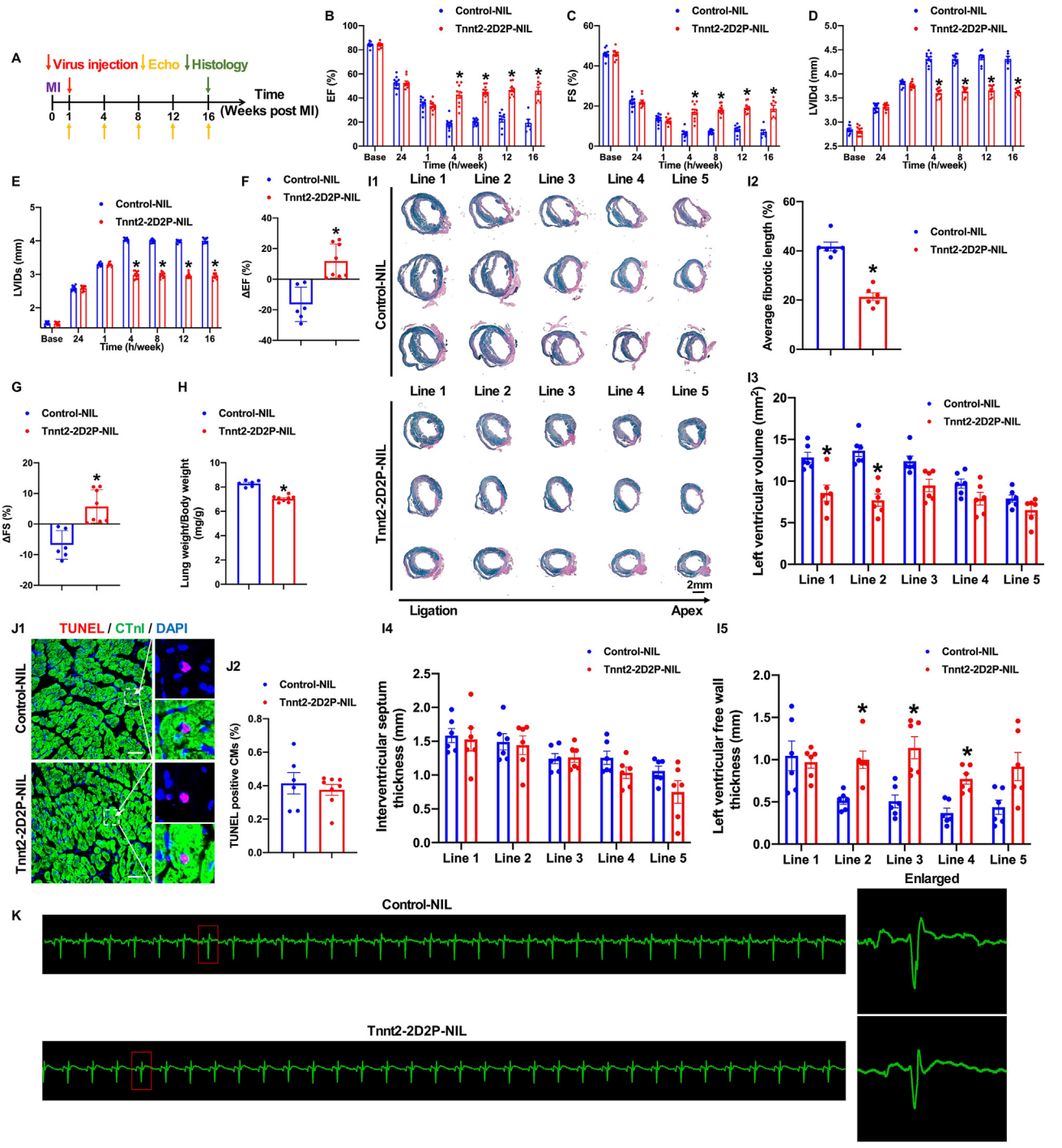

Figure 6 Tnnt2-2D2P-NIL treatment for 4 months results in a maintained improvement of cardiac function without obvious ventricular dilatation, thickened septum, or fatal arrhythmia. (A) Schematic diagram of the experimental design for the injection of Control-NIL or Tnnt2-2D2P-NIL viruses in mice. Echocardiographic analysis was performed at the age of 8 weeks as a baseline and 24 h, 1, 4, 8, 12, and 16 weeks after myocardial infarction (MI). Intramyocardial injection of the Tnnt2-2D2P-NIL or Control-NIL virus was performed 7 days after MI. (B−E) Quantification of left ventricular ejection fraction (EF%, B), fraction shortening (FS%, C), left ventricular internal diastolic diameter (LVIDd, D), and left ventricular internal systolic diameter (LVIDs, E). $n = 6-10$. $^*P < 0.05$ *vs.* Control-NIL. (F, G) Quantification of the change in EF% (ΔEF%, F) and FS% (ΔFS%, G) for each mouse between 1 and 16 weeks after MI. $n = 6-8$. $^*P < 0.05$ *vs.* Control-NIL. (H) Quantification of lung weight/body weight ratio in Control-NIL- or Tnnt2-2D2P-NIL-treated mice at 16 weeks after MI. $n = 6-8$. $^*P < 0.05$ *vs.* Control-NIL. (I) Serial sectioning was performed at 500 μm intervals from the ligation area to the apex. Representative images of Sirius red staining (I1) for the 5 lines in Control-NIL- or Tnnt2-2D2P-NIL-treated hearts at 16 weeks after MI. Scale bar, 2 mm. Quantification of fibrotic length (I2), left ventricular volume (I3), interventricular septum thickness (I4), and left ventricular free wall thickness (I5) by Sirius red staining 16 weeks after MI. $n = 5-6$. $^*P < 0.05$ *vs.* Control-NIL. (J) Representative images (J1) and quantification (J2) of the percentage of TUNEL$^+$ cardiomyocytes in Control-NIL- or Tnnt2-2D2P-NIL-treated hearts at 16 weeks after MI. Scale bar, 20 μm. $n = 6-8$. (K) Representative images of the electrocardiogram from Control-NIL- or Tnnt2-2D2P-NIL-treated mice at 16 weeks after MI.

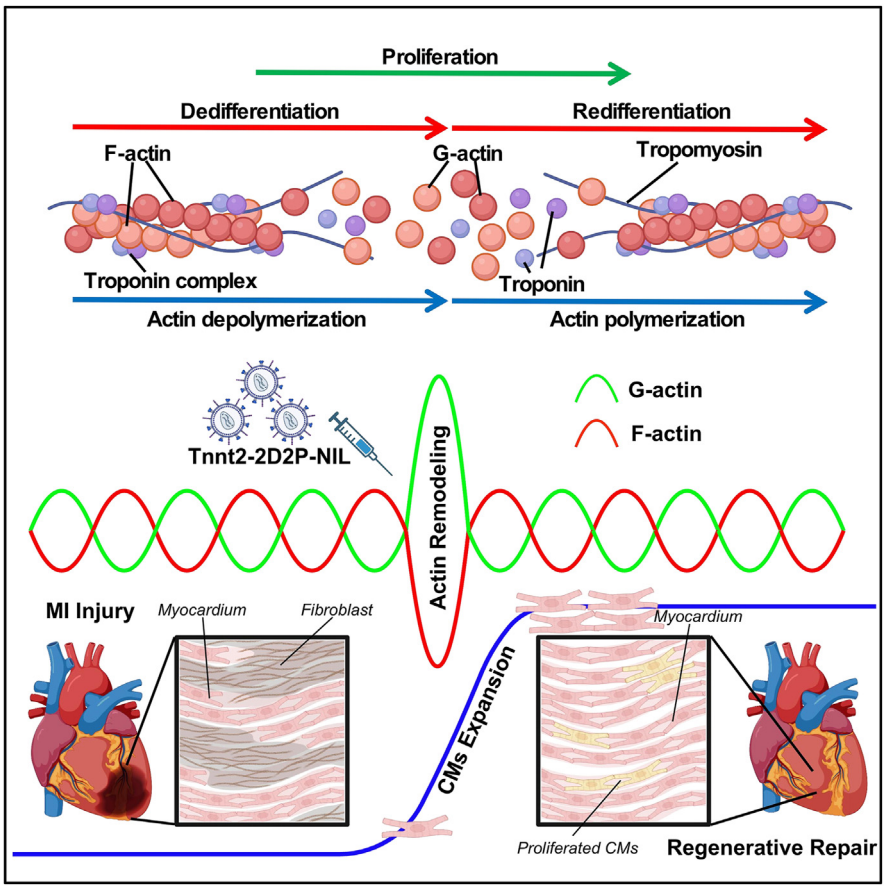

Figure 7 Actin cytoskeletal remodeling contributes to the dedifferentiation, proliferation, and redifferentiation of cardiomyocytes. Transient transfection of the 2D2P genes using Tnnt2-2D2P-NIL can promote cardiomyocyte expansion and regenerative repair after myocardial infarction.

transcription activity (Fig. S16D). This result implicated that Tnnt2-2D2P-NIL promoted F-actin and sarcomeric disassembly through the synergistic effect of Yap nuclear translocation and G-actin sequestration.

3.6. Tnnt2-2D2P-NIL treatment for 4 months resulted in a maintained improvement in cardiac function without obvious ventricular dilatation, thickened septum, or fatal arrhythmia

To evaluate the long-term efficacy and safety of Tnnt2-2D2P-NIL treatment *in vivo*, we permanently ligated the LAD in 8-week-old mice, followed by Tnnt2-2D2P-NIL injection 7 days after MI and a 16-week follow-up period (Fig. 6A). There was an improvement in cardiac function and reduction of ventricular dilatation with Tnnt2-2D2P-NIL treatment that was sustained from 4 to 16 weeks (Fig. 6B−E). Furthermore, there were significant improvements in ΔEF and ΔFS (between 1 week and 16 weeks) in the Tnnt2-2D2P-NIL-treated group compared with the Control-NIL group (Fig. 6F and G). Additionally, Tnnt2-2D2P-NIL injection significantly decreased the lung weight/body weight ratio, which was an indicator of heart failure (Fig. 6H)[33]. Consistent with the improvement in cardiac function, there was a significant reduction in infarct size that was still evident at 16 weeks after MI (Fig. 6I).

To avoid any potential confounding effects of comparing cardiac morphology across different relative positions, we analyzed the volume and thickness of the ventricles in each heart along five lines. The Tnnt2-2D2P-NIL treatment significantly decreased the left ventricular volume in lines 1 and 2 and significantly increased the thickness of the left ventricular free wall in lines 2−4, indicating the mitigation of ventricular dilatation and replacement of fibrosis with regenerated myocardium. There were no differences in interventricular septum thickness between the two groups across the five lines, suggesting that there was no long-term development of a thickened septum caused by Tnnt2-2D2P-NIL treatment (Fig. 6I). Furthermore, at 16 weeks after MI, there was no significant difference in cardiomyocyte apoptosis between the hearts treated with Tnnt2-2D2P-NIL and Control-NIL (Fig. 6J), and no episodes of ventricular arrhythmia, atrial fibrillation, or fatal arrhythmia were observed in either group (Fig. 6K). Moreover, Tnnt2-2D2P-NIL did not cause tumorigenesis in major organs, including the lung, liver, spleen, kidney, and skeletal muscle (Supporting Information Fig. S17).

4. Discussion

In this study, we aimed to investigate the role of actin remodeling in the dedifferentiation, proliferation, and redifferentiation of cardiomyocytes in neonatal and regenerating hearts after injury caused by MI. Our findings suggested that actin remodeling contributed to these processes and could be a potential approach for inducing cardiomyocyte proliferation in adult hearts after MI (Fig. 7). Specifically, we identified four top actin-remodeling regulators, namely *Tmsb4x*, *Tmsb10*, *Dmd*, and *Ctnna3*, collectively referred to as 2D2P. We demonstrated that transient changes in the expression of these genes efficiently induced proliferative activation in postnatal Day 7 cardiomyocytes and adult hearts.

Furthermore, intramyocardial delivery of Tnnt2-2D2P-NIL resulted in improved cardiac function without ventricular dilatation, thickened septum, or fatal arrhythmia.

MI injury in 1-day-old mice stimulates a drastic regenerative response, which is accompanied by sarcomeric disassembly/assembly, metabolic remodeling, immaturation/maturation, and dedifferentiation/redifferentiation in cardiomyocytes[1,34]. To better understand the regenerative process in neonates and to translate this knowledge to adults, we sought to identify the continuous trajectory of cardiac regeneration at a single-cell resolution level. Our findings suggested that actin remodeling contributed to the dedifferentiation, proliferation, and redifferentiation of cardiomyocytes, which was consistent with changes in immature and mature gene expressions. Actin filaments are the main axis of the thin myofibrils twined around by the troponin complex (T, C, and I)[35], and we hypothesized that the substantive characteristics of sarcomeric disassembly/assembly may be actin remodeling. Previous studies have shown that modulation of sarcomeric disassembly is an effective approach to induce cardiomyocyte mitosis/cytokinesis through Agrin/dystrophin glycoprotein complex[36], Yap/Hippo[37], or Meis1/Hoxb13[38] pathways. We further demonstrated that four crucial genes (*Dmd*, *Ctnna3*, *Tmsb4x*, and *Tmsb10*) driving actin remodeling, named 2D2P, were conspicuously changed in the regenerative trajectory. *Dmd* encodes dystrophin, a component of the dystrophin glycoprotein complex that bridges the inner cytoskeleton and the extracellular matrix by directly binding to F-actin[39]. Mice persistently lacking dystrophin (Mdx) show elevated cardiomyocyte proliferation ability but fail to regenerate myocardium after apical resection due to disabled actin cytoskeletal remodeling and absent protrusion formation[29,40]. Combined with our previous studies, we hypothesized that the reason for the regeneration deficiency in Mdx mice was the impairment of cardiomyocyte redifferentiation caused by a persistent lack of dystrophin. In addition, α-catenins functionally link intercalated discs and the F-actins[41,42]. Double cardiac-specific knockout of *Ctnna1* (Catenin α1) and *Ctnna3* (Catenin α3) can increase cardiomyocyte proliferation and improve cardiac function after MI, which is accompanied by less mature cardiac gene expression[30]. The actin-binding Thymosin β4 (*Tmsb4x*) and Thymosin β10 (*Tmsb10*) play an important role in the organization of the actin cytoskeleton, binding to and sequestering G-actin, thereby inhibiting actin polymerization[43]. A recent study showed that a combination of Thymosin β4 and prothymosin alpha can provide a permissive environment for cardiomyocyte proliferation and thereby attenuate cardiac dysfunction[44]. Thus, altered expression of the 2D2P genes may recapitulate the process of actin remodeling in cardiac regeneration.

Although manipulating a single gene is sufficient to promote cardiac regeneration and repair, an increasing number of studies are focusing on the combined intervention of multiple genes or targets for more significant effects on cardiomyocyte proliferation. For instance, a chemical cocktail of five small molecules promotes adult cardiomyocyte proliferation and heart regeneration by inducing a metabolic switch toward glycolysis/biosynthesis and dedifferentiation[45]. Short-term cardiac-specific expression of *Oct4*, *Sox2*, *Klf4*, and *c-Myc* induces adult cardiomyocytes to dedifferentiate, conferring regenerative capacity to adult hearts[46]. Moreover, transient overexpression of *Cdk1*, *Ccnb1*, *Cdk4*, and *Ccnd1* using NIL revealed that 15% of adult cardiomyocytes undergo stable cell division, with significant improvement in cardiac function after acute or subacute MI[47,33]. In our study, we found that Tnnt2-2D2P-NIL treatment induced transient actin remodeling and expansion of cardiomyocytes, resulting in improved cardiac function and reduced scar size in mice after MI. After four months of treatment, Tnnt2-2D2P-NIL maintained the improvement in cardiac function without obvious ventricular dilatation, thickened septum, or fatal arrhythmia. Our findings provided insights into the critical role of actin remodeling in sarcomere disassembly and assembly, coupled with cardiomyocyte dedifferentiation, proliferation, and redifferentiation.

The sarcomeric disassembly is often used as an important marker of dedifferentiated cardiomyocytes with enhanced regenerative capacity[36,45]. In our study, we found that F-actin acted as the main axis of the thin myofibrils of the sarcomere, and the depolymerization of F-actin was the essence of the sarcomeric disassembly during the proliferation of cardiomyocytes. Therefore, our mechanistic experiments focused on how the 2D2P genes acted together to cause F-actin depolymerization and sarcomere disassembly. Previous studies show that enhanced Yap nuclear translocation and sarcomeric disassembly are associated with the inactivation of both Dystrophin and Catenin α3[29,30]. Additionally, as G-actin isolators, Thymosin β4 and Thymosin β10 inhibit the polymerization of G-actin by binding to the "LKKTET" site of G-actin in a 1:1 ratio through conformational and spatial effects, thereby they can control the threshold concentration of G-actin in the cytoplasm, influence the balance of depolymerization and polymerization of F-actin[32]. In the present study, we found Yap inhibitor and "LKKTET" truncated Thymosin β4/Thymosin β10 could block the effect of Tnnt2-2D2P-NIL on cardiomyocyte proliferation, F-actin and sarcomeric disassembly, which suggested the synergistic and incorporative effect of 2D2P genes.

However, our study has some limitations. First, we used NIL to simulate the up- and down-regulation of 2D2P genes in temporal and spatial patterns, but we could not control the absolute quantity of the changes in gene expression. Second, the regenerative effect of Tnnt2-2D2P-NIL needs to be verified in large animals, which have larger hearts that would have better clinical translation value. Third, although *Aurkb* is a marker of cytokinesis, the *Aurkb*-rox-RFP/*Tnnt2*-Dre reporter overestimates cytokinesis events[33], and the Cre-recombinase-dependent MADM lineage tracing system underestimates cytokinesis events[27].

5. Conclusions

Our study highlights the importance of actin remodeling in sarcomere disassembly and assembly, coupled with cardiomyocyte dedifferentiation, proliferation, and redifferentiation, in cardiac regeneration. We hope that our findings provide a foundation for future research exploring actin remodeling as an approach to drive proliferation in organs that have limited regenerative capacity.

Acknowledgments

This study was supported by the grant to Chunyu Zeng from the National Key R&D Program of China (2022YFA1104500), by the grant to Wenbin Fu from the National Natural Science Foundation of China (82200307), and by the grant to Chunyu Zeng from the National Natural Science Foundation of China (81930008).

Author contributions

Wenbin Fu performed experiments, analyzed data, and wrote the paper. Chunyu Zeng supervised experiments, analyzed data, and edited the paper. Qiao Liao, Wujian Liu, Yu Shi, Hongmei Ren, and

Chunmei Xu carried out experiments and analyzed the data. All authors revised the manuscript and approved the final version.

Conflicts of interest

The authors declare that they have no conflicts of interest.

Appendix A. Supporting information

Supporting data to this article can be found online at https://doi.org/10.1016/j.apsb.2024.01.021.

References

1. Costa A, Cushman S, Haubner BJ, Derda AA, Thum T, Bär C. Neonatal injury models: integral tools to decipher the molecular basis of cardiac regeneration. *Basic Res Cardiol* 2022;**117**:26.
2. Fu W, Ren H, Shou J, Liao Q, Li L, Shi Y, et al. Loss of NPPA-AS1 promotes heart regeneration by stabilizing SFPQ-NONO heteromer-induced DNA repair. *Basic Res Cardiol* 2022;**117**:10.
3. He L, Nguyen NB, Ardehali R, Zhou B. Heart regeneration by endogenous stem cells and cardiomyocyte proliferation: controversy, fallacy, and progress. *Circulation* 2020;**142**:275−91.
4. Senyo SE, Steinhauser ML, Pizzimenti CL, Yang VK, Cai L, Wang M, et al. Mammalian heart renewal by pre-existing cardiomyocytes. *Nature* 2013;**493**:433−6.
5. Wang WE, Li L, Xia X, Fu W, Liao Q, Lan C, et al. Dedifferentiation, proliferation, and redifferentiation of adult mammalian cardiomyocytes after ischemic injury. *Circulation* 2017;**136**:834−48.
6. Cui M, Wang Z, Chen K, Shah AM, Tan W, Duan L, et al. Dynamic transcriptional responses to injury of regenerative and non-regenerative cardiomyocytes revealed by single-nucleus RNA sequencing. *Dev Cell* 2020;**53**:102−116.e8.
7. Kuzmin DA, Shutova MV, Johnston NR, Smith OP, Fedorin VV, Kukushkin YS, et al. The clinical landscape for AAV gene therapies. *Nat Rev Drug Discov* 2021;**20**:173−4.
8. Gabisonia K, Prosdocimo G, Aquaro GD, Carlucci L, Zentilin L, Secco I, et al. MicroRNA therapy stimulates uncontrolled cardiac repair after myocardial infarction in pigs. *Nature* 2019;**569**:418−22.
9. Pereira AHM, Cardoso AC, Franchini KG. Isolation, culture, and immunostaining of neonatal rat ventricular myocytes. *STAR Protoc* 2021;**2**:100950.
10. Sui W, Zhang D. Four methods for roundness evaluation. *Phys Procedia* 2012;**24**:2159−64.
11. Fu W, Liao Q, Li L, Shi Y, Zeng A, Zeng C, et al. An aurora kinase B-based mouse system to efficiently identify and analyze proliferating cardiomyocytes. *Front Cell Dev Biol* 2020;**8**:570252.
12. Hao Y, Hao S, Andersen-Nissen E, Mauck WM, Zheng S, Butler A, et al. Integrated analysis of multimodal single-cell data. *Cell* 2021;**184**:3573−3587.e29.
13. Korsunsky I, Millard N, Fan J, Slowikowski K, Zhang F, Wei K, et al. Fast, sensitive and accurate integration of single-cell data with harmony. *Nat Methods* 2019;**16**:1289−96.
14. Cao J, Spielmann M, Qiu X, Huang X, Ibrahim DM, Hill AJ, et al. The single-cell transcriptional landscape of mammalian organogenesis. *Nature* 2019;**566**:496−502.
15. Jopling C, Sleep E, Raya M, Martí M, Raya A, Izpisúa Belmonte JC. Zebrafish heart regeneration occurs by cardiomyocyte dedifferentiation and proliferation. *Nature* 2010;**464**:606−9.
16. Dominguez R, Holmes KC. Actin structure and function. *Annu Rev Biophys* 2011;**40**:169−86.
17. Guhathakurta P, Carter AL, Thompson AR, Kurila D, LaFrence J, Zhang L, et al. Enhancing interaction of actin and actin-binding domain 1 of dystrophin with modulators: toward improved gene therapy for Duchenne muscular dystrophy. *J Biol Chem* 2022;**298**:102675.
18. Meng X, Jiang Q, Chang N, Wang X, Liu C, Xiong J, et al. Small activating RNA binds to the genomic target site in a seed-region-dependent manner. *Nucleic Acids Res* 2016;**44**:2274−82.
19. van Gorp PRR, Zhang J, Liu J, Tsonaka R, Mei H, Dekker SO, et al. Sbk2, a newly discovered atrium-enriched regulator of sarcomere integrity. *Circ Res* 2022;**131**:24−41.
20. Porrello ER, Mahmoud AI, Simpson E, Johnson BA, Grinsfelder D, Canseco D, et al. Regulation of neonatal and adult mammalian heart regeneration by the miR-15 family. *Proc Natl Acad Sci U S A* 2013;**110**:187−92.
21. Puente BN, Kimura W, Muralidhar SA, Moon J, Amatruda JF, Phelps KL, et al. The oxygen-rich postnatal environment induces cardiomyocyte cell-cycle arrest through DNA damage response. *Cell* 2014;**157**:565−79.
22. Xu Z, Chen F, Zhang L, Lu J, Xu P, Liu G, et al. Non-integrating lentiviral vectors based on the minimal S/MAR sequence retain transgene expression in dividing cells. *Sci China Life Sci* 2016;**59**:1024−33.
23. Nightingale SJ, Hollis RP, Pepper KA, Petersen D, Yu XJ, Yang C, et al. Transient gene expression by nonintegrating lentiviral vectors. *Mol Ther* 2006;**13**:1121−32.
24. Shaw A, Cornetta K. Design and potential of non-integrating lentiviral vectors. *Biomedicines* 2014;**2**:14−35.
25. Milone MC, O'Doherty U. Clinical use of lentiviral vectors. *Leukemia* 2018;**32**:1529−41.
26. Mohamed TM, Stone NR, Berry EC, Radzinsky E, Huang Y, Pratt K, et al. Chemical enhancement of *in vitro* and *in vivo* direct cardiac reprogramming. *Circulation* 2017;**135**:978−95.
27. Ali SR, Hippenmeyer S, Saadat LV, Luo L, Weissman IL, Ardehali R. Existing cardiomyocytes generate cardiomyocytes at a low rate after birth in mice. *Proc Natl Acad Sci U S A* 2014;**111**:8850−5.
28. Henson JH. Relationships between the actin cytoskeleton and cell volume regulation. *Microsc Res Tech* 1999;**47**:155−62.
29. Morikawa Y, Heallen T, Leach J, Xiao Y, Martin JF. Dystrophin−glycoprotein complex sequesters Yap to inhibit cardiomyocyte proliferation. *Nature* 2017;**547**:227−31.
30. Li J, Gao E, Vite A, Yi R, Gomez L, Goossens S, et al. Alpha-catenins control cardiomyocyte proliferation by regulating Yap activity. *Circ Res* 2015;**116**:70−9.
31. Matsui Y, Lai ZC. Mutual regulation between Hippo signaling and actin cytoskeleton. *Protein Cell* 2013;**4**:904−10.
32. Ying Y, Lin C, Tao N, Hoffman RD, Shi D, Chen Z, et al. Thymosin β4 and actin: binding modes, biological functions and clinical applications. *Curr Protein Pept Sci* 2023;**24**:78−88.
33. Abouleisa RRE, Salama ABM, Ou Q, Tang XL, Solanki M, Guo Y, et al. Transient cell cycle induction in cardiomyocytes to treat subacute ischemic heart failure. *Circulation* 2022;**145**:1339−55.
34. Yuan X, Braun T. Multimodal regulation of cardiac myocyte proliferation. *Circ Res* 2017;**121**:293−309.
35. Gordon AM, Homsher E, Regnier M. Regulation of contraction in striated muscle. *Physiol Rev* 2000;**80**:853−924.
36. Bassat E, Mutlak YE, Genzelinakh A, Shadrin IY, Baruch Umansky K, Yifa O, et al. The extracellular matrix protein agrin promotes heart regeneration in mice. *Nature* 2017;**547**:179−84.
37. Monroe TO, Hill MC, Morikawa Y, Leach JP, Heallen T, Cao S, et al. Yap partially reprograms chromatin accessibility to directly induce adult cardiogenesis *in vivo*. *Dev Cell* 2019;**48**:765−779.e7.
38. Nguyen NUN, Canseco DC, Xiao F, Nakada Y, Li S, Lam NT, et al. A calcineurin−Hoxb13 axis regulates growth mode of mammalian cardiomyocytes. *Nature* 2020;**582**:271−6.
39. Valera IC, Wacker AL, Hwang HS, Holmes C, Laitano O, Landstrom AP, et al. Essential roles of the dystrophin−glycoprotein complex in different cardiac pathologies. *Adv Med Sci* 2021;**66**:52−71.
40. Morikawa Y, Zhang M, Heallen T, Leach J, Tao G, Xiao Y, et al. Actin cytoskeletal remodeling with protrusion formation is essential for heart regeneration in Hippo-deficient mice. *Sci Signal* 2015;**8**. ra41.
41. Vite A, Zhang C, Yi R, Emms S, Radice GL. α-Catenin-dependent cytoskeletal tension controls Yap activity in the heart. *Development* 2018;**145**:dev149823.

42. Arbore C, Sergides M, Gardini L, Bianchi G, Kashchuk AV, Pertici I, et al. α-Catenin switches between a slip and an asymmetric catch bond with F-actin to cooperatively regulate cell junction fluidity. *Nat Commun* 2022;**13**:1146.
43. Yu FX, Lin SC, Morrison-Bogorad M, Atkinson MA, Yin HL. Thymosin beta 10 and thymosin beta 4 are both actin monomer sequestering proteins. *J Biol Chem* 1993;**268**:502−9.
44. Gladka MM, Johansen AKZ, van Kampen SJ, Peters MMC, Molenaar B, Versteeg D, et al. Thymosin β4 and prothymosin α promote cardiac regeneration post-ischemic injury in mice. *Cardiovasc Res* 2023;**119**:802−12.
45. Du J, Zheng L, Gao P, Yang H, Yang WJ, Guo F, et al. A small-molecule cocktail promotes mammalian cardiomyocyte proliferation and heart regeneration. *Cell Stem Cell* 2022;**29**:545−558.e13.
46. Chen Y, Lüttmann FF, Schoger E, Schöler HR, Zelarayán LC, Kim KP, et al. Reversible reprogramming of cardiomyocytes to a fetal state drives heart regeneration in mice. *Science* 2021;**373**:1537−40.
47. Mohamed TMA, Ang YS, Radzinsky E, Zhou P, Huang Y, Elfenbein A, et al. Regulation of cell cycle to stimulate adult cardiomyocyte proliferation and cardiac regeneration. *Cell* 2018;**173**:104−116.e12.